Title
Copper regulates rest-activity cycles through the locus coeruleus-norepinephrine system.

Journal
Nature chemical biology, 14(7)

ISSN
1552-4450

Authors
Xiao, Tong
Ackerman, Cheri M
Carroll, Elizabeth C
et al.

Publication Date
2018-07-01

DOI
10.1038/s41589-018-0062-z

Peer reviewed

nature chemical biology

ARTICLES

https://doi.org/10.1038/s41589-018-0062-z

Copper regulates rest-activity cycles through the locus coeruleus-norepinephrine system

Tong Xiao[1,2], Cheri M. Ackerman[1,2], Elizabeth C. Carroll[3,5], Shang Jia[1,2], Adam Hoagland[3], Jefferson Chan[1,2], Bao Thai[2,3], Christine S. Liu[1,2], Ehud Y. Isacoff[3,4] and Christopher J. Chang[1,2,3,4]*

The unusually high demand for metals in the brain, along with insufficient understanding of how their dysregulation contributes to neurological diseases, motivates the study of how inorganic chemistry influences neural circuitry. We now report that the transition metal copper is essential for regulating rest–activity cycles and arousal. Copper imaging and gene expression analysis in zebrafish identifies the locus coeruleus–norepinephrine (LC-NE) system, a vertebrate-specific neuromodulatory circuit critical for regulating sleep, arousal, attention, memory and emotion, as a copper-enriched unit with high levels of copper transporters CTR1 and ATP7A and the copper enzyme dopamine β-hydroxylase (DBH) that produces NE. Copper deficiency induced by genetic disruption of ATP7A, which loads copper into DBH, lowers NE levels and hinders LC function as manifested by disruption in rest–activity modulation. Moreover, LC dysfunction caused by copper deficiency from ATP7A disruption can be rescued by restoring synaptic levels of NE, establishing a molecular CTR1–ATP7A–DBH–NE axis for copper-dependent LC function.

For reasons that remain insufficiently understood, the unique biology of the brain as the center of consciousness is underpinned by its unique chemistry involving accumulating select elements at higher concentrations than anywhere else in the body[1,2]. These include redox-active transition metals such as copper and iron[2], in part because the brain is the body's most oxidatively active organ, comprising just 2% of body weight but requiring 20% of oxygen consumption. However, the brain's dependence on metals for normal function may be a double-edged sword, as the same potent redox activity of copper and iron can trigger oxidative stress and damage, leading to neurodegeneration[2–7].

Copper distribution in the brain is spatially diverse and changes with age and nutritional status[8]. In the human brain, the LC acquires ~10 times higher copper concentrations than other brain regions[2,9,10] and is particularly vulnerable in many neurodegenerative diseases, including Alzheimer's, Parkinson's and Huntington's diseases[11–13]. At the cellular level, copper pools are regulated by several copper transporters[14,15], including the high affinity copper transporter, CTR1 (also known as SLC31A1), as well as metallochaperones that deliver copper to various destinations within the cytosol and organelles[16–18]. In this context, the copper-dependent ATPases ATP7A and ATP7B serve the dual purpose of metalating proteins and/or controlling copper efflux from the cell[4,19]. Despite advances in the field, molecular and cellular mechanisms of how homeostatic control of brain copper influences behavior remain insufficiently understood.

To study how transition metals are used in the brain, we focused on the copper-rich LC region, which has broad projections throughout the central nervous system. In mammals, the LC is believed to regulate sleep, arousal, learning, attention, mood and fear responses[20,21]. The chemistry of the LC is dominated by catecholamines, and their imbalance contributes to severe psychiatric disorders[22]. The two catecholamines present in the LC, dopamine (DA) and norepinephrine (NE), share a common biosynthetic pathway, up to a final step during which the copper-dependent enzyme DBH[23–25] converts DA to NE. DBH is metalated by the P-type copper-transporting ATPase ATP7A[26]. The LC is the main source of NE to the central nervous system (CNS), and levels of NE in the mammalian brain are higher than those of DA, even though DA neurons greatly outnumber their NE counterparts[27]. Unlike DA and serotonin (5-hydroxytrypamine, 5-HT), NE is unique to vertebrates[28–30]; however, when the LC-NE system emerged during evolution remains unclear.

Against this backdrop, we used zebrafish as a model organism to study metal-dependent brain chemistry. Here we report an essential role for copper in the brain in regulating sleep-related and arousal behaviors through the LC-NE system. Metal imaging studies using a pair of newly developed fluorescent copper probes along with laser ablation inductively coupled plasma mass spectrometry (LA-ICP-MS) reveal enrichment of copper in brain neurites and neuropils rather than cell bodies. Complementary in situ hybridization studies showed high levels of copper transporters CTR1 and ATP7A, along with the copper enzyme DBH, localized to the LC. Copper deficiency induced by genetic manipulation of ATP7A showed that this metal is critical for LC-mediated rest–activity balance and arousal response and that this effect is associated with regulation of synaptic NE, the product of copper-dependent DBH catalysis. Phylogenetic analysis showed that development of the LC-NE is assisted by evolution of more specialized copper transporters in Gnathostomata through gene duplication of ATP7 into ATP7A and ATP7B. Taken together, the data identify an essential role for copper in the evolution and function of the LC-NE through a molecular CTR1–ATP7A–DBH–NE axis, including a role for copper in the regulation of sleep-related and arousal behaviors.

Results

Imaging labile copper in the zebrafish brain. As a starting point for our investigations, we sought to visualize distributions of labile copper within the brains of these living organisms, as previous in vivo copper imaging studies were limited primarily to liver detection[31,32]. To meet this goal, we designed and synthesized

[1]Department of Chemistry, University of California, Berkeley, CA, USA. [2]Howard Hughes Medical Institute, University of California, Berkeley, CA, USA. [3]Department of Molecular and Cell Biology, University of California, Berkeley, CA, USA. [4]Helen Wills Neuroscience Institute, University of California, Berkeley, CA, USA. Present address: [5]Department of Imaging Physics, Delft University of Technology, Delft, The Netherlands.
*e-mail: chrischang@berkeley.edu

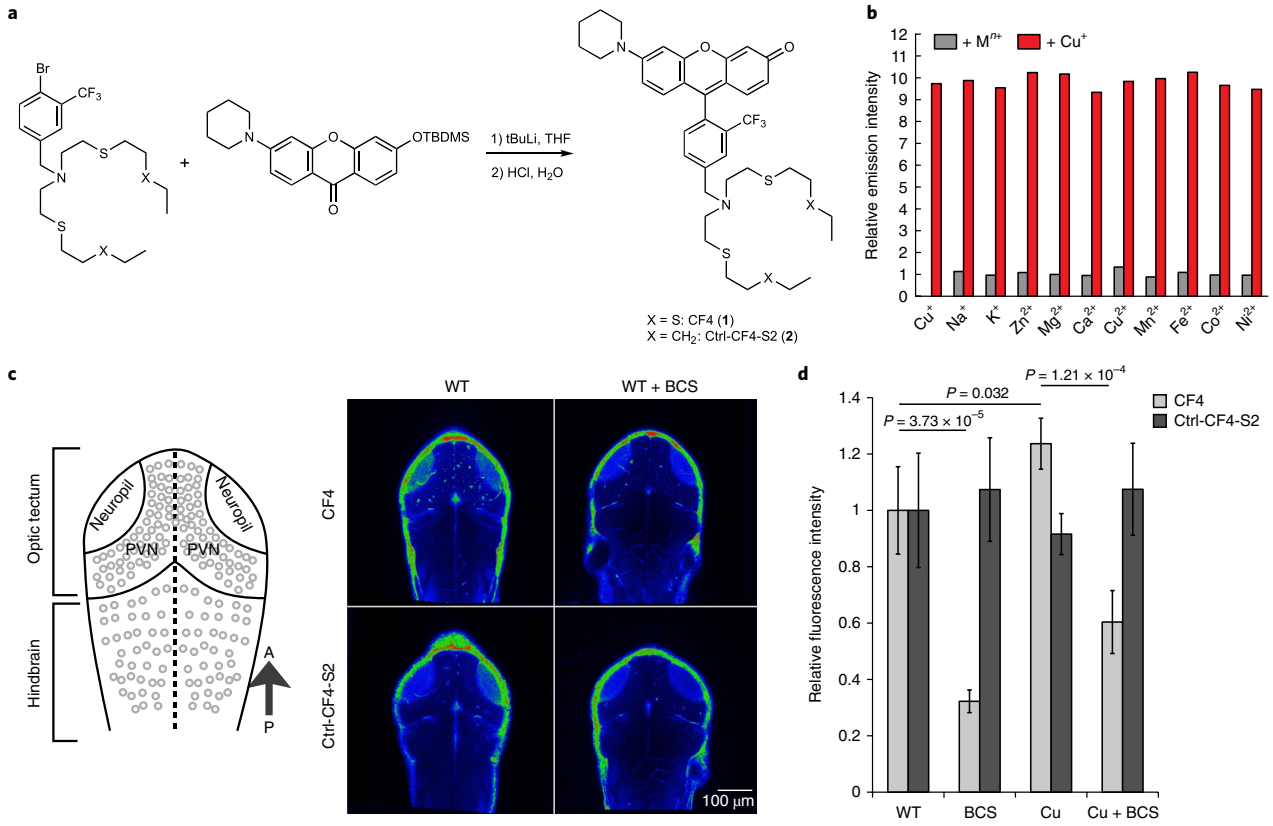

Fig. 1 | Molecular imaging reveals distributions of labile copper in the living brain. a, The synthesis of CF4 (**1**) and control probe Ctrl-CF4-S2 (**2**). **b**, Fluorescence responses of CF4 to various metal ions. Bars represent the final integrated fluorescence response (F_f) over the initial integrated emission (F_i). Gray bars represent the addition of an excess of the appropriate metal (M) ion (2 mM for Na^+, Mg^{2+}, K^+, Ca^{2+} and Zn^{2+}, 50 µM for all other cations) to a 2 µM solution of CF4. Red bars represent the subsequent addition of 2.5 µM Cu^+ to the solution. **c**, CF4 and Ctrl-CF4-S2 signals in 3 dpf zebrafish brain. PVN, periventricular neurons. In the optic tectum, the PVN zone consists mostly of tectal neurons' cell bodies while the neuropil consists mostly of neurites from retinal ganglion cells, tectal neurons and other neurons with input to visual signal processing. P → A, posterior to anterior. These experiments have been repeated independently 3 times with similar results. WT, wild type. **d**, Quantification of CF4 and Ctrl-CF4-S2 signals in the tectum region. $N = 12$ fish for each group. Bars represent mean ± s.e.m. Two-sided Student's *t*-tests.

Copper Fluor-4 (CF4; **1**) and Control Copper Fluor-4 Sulfur 2 (Ctrl-CF4-S2; **2**), a pair of molecular probes that, when used in concert, can enable detection of labile copper pools in small living organisms (Fig. 1a). CF4 is a Cu^+-specific fluorescent sensor based on a rhodol dye scaffold that displays a tenfold increase in fluorescence in response to copper; is stable in a physiologically relevant pH regime between 6 and 8 (Supplementary Fig. 1); has high copper selectivity, particularly over zinc and iron, as well as abundant cellular alkali and alkaline earth metals (Fig. 1b); and has a 1:1 Cu^+:probe binding stoichiometry and an apparent K_d of 2.9×10^{-13} M (Supplementary Fig. 2 and Supplementary Table 1). The introduction of a six-membered piperidine group on the xanthenone ring of the rhodol affords a probe with good cellular retention and high signal-to-noise ratio to image copper within whole living organisms.

A key chemical advance lay in the development of Ctrl-CF4-S2, which utilizes the same dye scaffold as CF4 but does not respond to copper owing to its modified isosteric receptor (Supplementary Fig. 3). Like previously reported control probes for labile copper imaging in cells, Ctrl-CF4-S2 is comparable in size, shape and hydrophobicity to its parent copper probe CF4. However, a subtle but important chemical difference that enables the expansion of this concept to in vivo use is that just two of the four thioether ligands in the copper-responsive CF4 receptor are replaced with methylene groups, rather than changing all four sulfur donors to carbons as reported in previous designs. The resulting Ctrl-CF4-S2 compound bears an NS_2C_2 receptor that exhibits greater in vivo permeability for use in living organisms (Supplementary Fig. 4). Indeed, the analogous Control Copper Fluor-4 (Ctrl-CF4, **9**) compound with an NC_4 receptor does not penetrate beyond the skin of zebrafish, while the new Ctrl-CF4-S2 control dye permeates the fish and shows comparable in vivo distribution to the parent CF4 indicator (Supplementary Fig. 4). The uptake ratio of CF4 and Ctrl-CF4-S2 in live zebrafish is comparable to that in HEK cells, a standard cell model for evaluating fluorescent probes (Supplementary Fig. 5).

We then applied CF4 and Ctrl-CF4-S2 to visualize labile copper pools in developing zebrafish embryos (Fig. 1c). The CF4 signal appeared strongly associated with neuropils, extracellular matrix and ventricles, but was excluded from the nuclei of cells. Copper supplementation of fish with 100 µM copper(II) dihistidine complex for 30 min resulted in a statistically significant increase in CF4 fluorescence while copper deficiency induced by overnight treatment of fish with the copper chelator bathocuproine disulfonate (BCS) at 500 µM decreased the CF4 signal (Fig. 1d). In both HEPES buffer and cell lysates, CF4 showed strong dose-dependent responses to copper (Supplementary Figs. 6 and 7). In contrast, we observed no significant changes in Ctrl-CF4-S2 fluorescent signals with either copper(II) dihistidine complex or BCS addition (Fig. 1d), suggesting that labile pools of copper in the developing zebrafish brain are

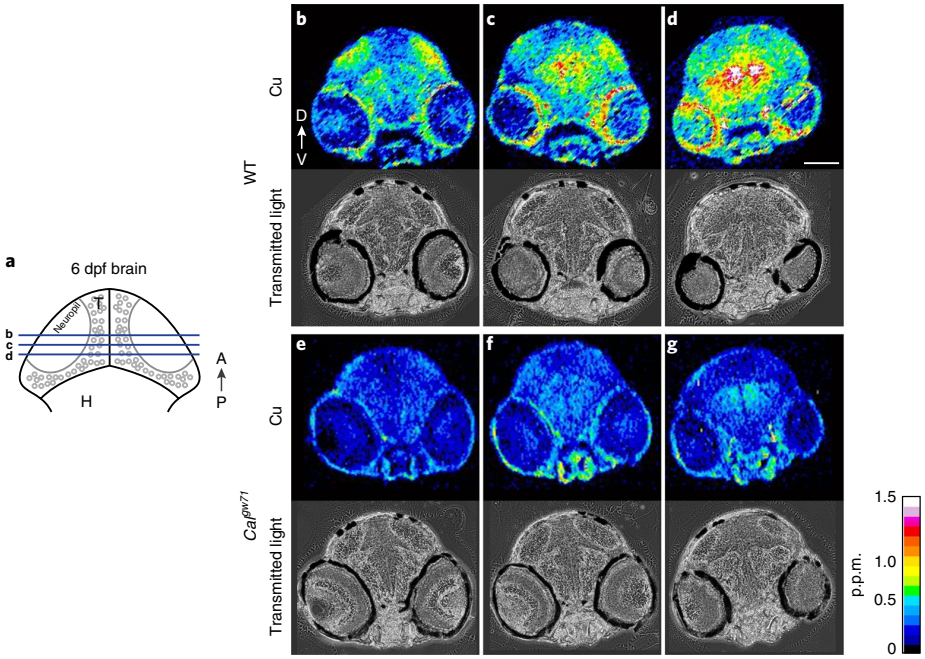

Fig. 2 | LA-ICP-MS imaging reveals heterogeneous copper distribution patterns in the brain during development. a, At 6 dpf, neurites innervate most brain regions. The lines indicate the three consecutive sections shown in **b**–**d**. **b**–**d**, Copper distributions measured by LA-LCP-MS of 6 dpf wild-type (WT) controls, in the sections indicated by the lines in **a**. **e**–**g**, Consecutive sections (analogous to **b**–**d**) of LA-ICP-MS images of 6-dpf *Cal*^{gw71} mutants. Scale bar is 100 µm. T, tectum; H, hindbrain; P → A, posterior to anterior; V → D, ventral to dorsal. The colorimetric scale bar represents copper concentrations ranging from 0 to 1.5 p.p.m. $N = 6$ independent animals imaged for each genotype with similar results.

localized to neural processes and brain ventricles. Taken together, the data establish that CF4 and Ctrl-CF4-S2 can be used in concert to assess changes in labile copper distributions in small living organisms such as zebrafish and that subtle design changes in receptors can create effective control probe and probe pairs for in vivo use.

A dynamic copper distribution in the developing brain. To provide a more direct measure of copper distributions in the developing zebrafish brain, we employed LA-ICP-MS[33,34] on flash-frozen tissues to map total brain copper pools with spatial resolution (Fig. 2 and Supplementary Fig. 8). These studies reveal that copper distribution is spatially and temporally regulated in the developing zebrafish brain, with copper concentrations varying among brain regions and steadily rising throughout development. In line with previous studies in rodents suggesting that brain copper is concentrated in the neuropil within synaptic vesicles[35–37], we observed elevated copper levels in larvae and adults in neuropils and fascicles, rather than somata of neurons (Supplementary Fig. 9). Moreover, these data are consistent with CF4 and Ctrl-CF4-S2 molecular imaging of labile copper pools. As a representative example illustrating the dynamic nature of brain copper distributions during development, we focused on the tectal neuropil, which is the largest neuropil containing a high density of neurites. We analyzed the copper signals at developmental stages before and after neurite innervation and found that copper levels in the tectum were low (<0.5 p.p.m.) at 2 days post fertilization (dpf), a developmental time point at which no neurites have reached this region (Supplementary Fig. 8), and rose in concert with progressive neurite innervation at 4 dpf (Supplementary Fig. 8) and 6 dpf (Fig. 2a–d), reaching 1.5 p.p.m. copper. In contrast, analogous LA-ICP-MS imaging of zinc showed the opposite cellular distribution to copper, with highest observed zinc levels concentrated within cell bodies and little detectable signal in neuropils or fascicles (Supplementary Fig. 10).

The ATP7A mutant has reduced copper levels in the brain. To study how copper regulates brain function, we employed a genetic model of copper dysregulation, *Calamity*$^{gw71/gw71}$ (*Cal*^{gw71}). *Cal*^{gw71} mutants, bearing a hypomorphic allele of the *atp7a* gene[38], are morphologically indistinguishable from their wild-type siblings under normal rearing conditions—embryo medium or system water reconstituted from instant ocean salt, which contains approximately 1.8 µmol/kg of copper (Methods). Notably, LA-ICP-MS copper mapping established that not only were overall brain copper levels lower in *Cal*^{gw71} fish compared to their wild-type counterparts (Fig. 2e–g and Supplementary Fig. 8), but dramatic decreases were observed in neuropil and fascicle regions ($P < 0.001$ at 4 dpf and 6 dpf quantified in the tectal neuropil, $N = 18$ for each group). This copper deficiency is spatially selective, as total larval copper concentrations in *Cal*^{gw71} (0.87 µg copper/g tissue) vs. wild-type (0.92 µg copper/g tissue) fish at 5–6 dpf were comparable, suggesting that reduction of ATP7A function causes selective disruption in copper accumulation in the brain. In contrast, zinc levels in *Cal*^{gw71} mutants remained unchanged from wild type (Supplementary Fig. 11).

Copper modulates rest–activity cycles. Next, we investigated changes in the labile copper pool in *Cal*^{gw71} mutants with CF4 (Fig. 3a and Supplementary Fig. 12). As in larvae treated with the copper chelator BCS, we observed decreases in CF4 fluorescence signals in the brains of *Cal*^{gw71} mutants compared to wild-type controls. Having characterized brain copper pools in developing zebrafish through a combination of labile copper and total copper imaging using molecular probes and LA-ICP-MS, respectively, we next evaluated functions of this metal in neural circuitry. In particular, we explored the potential contributions of copper to arousal behaviors in simple model organisms, inspired by the insufficiently understood rest–wake disorders observed in some patients with genetic disorders of copper metabolism[39].

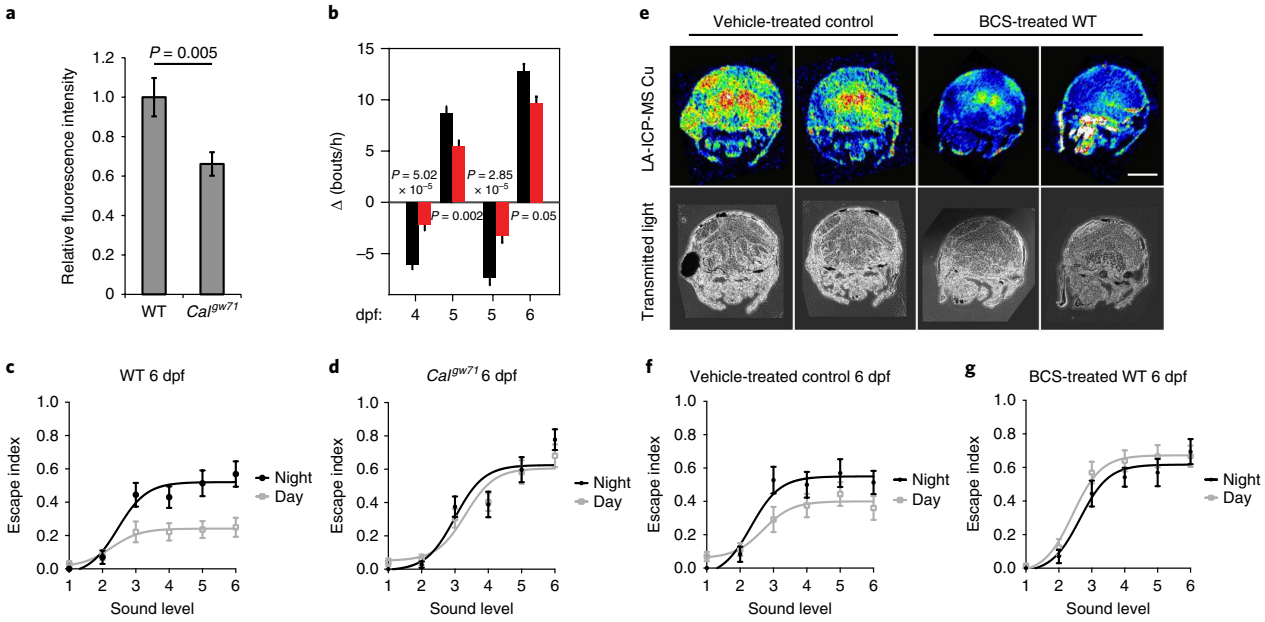

Fig. 3 | Dysregulation of brain copper homeostasis alters arousal and rest–activity behavior. a, Quantification of CF4 fluorescence signal intensity in brain of wild-type (WT) larvae and *Cal*^{gw71} mutants. $N=12$ brains for each group. Bars represent mean ± s.e.m. Two-sided Student's *t*-test. **b**, Change in frequency of swim bouts in WT (black, $n=98$) and *Cal*^{gw71} mutants (red, $n=99$) from 5 to 6 dpf. Change in frequency of swim bouts recorded in 3-h period preceding and following light transitions at dusk and dawn. Bars represent mean ± s.e.m. Two-sided Student's *t*-test. **c**, Comparison of stimulus–response curves to sound using ASR assay at night (black line) and day (gray line) in WT ($n=24$). $P<0.0001$ by extra sum-of-squares *F* test. The escape index is the response probability calculated by the percentage of fish displaying movements to sound stimulus. **d**, Comparison of stimulus–response curves to sound at night (black line) and day (gray line) of *Cal*^{gw71} mutants ($n=24$). $P=0.1$ by extra sum-of-squares *F* test. Bars represent mean ± s.e.m. **c** and **d** were tested with 6 dpf larvae. **e**, LA-ICP-MS images of copper distribution of 6 dpf larval brain sections, showing that BCS-treated larvae have decreased brain copper compared to their control group. $N=6$ for each group. Scale bar, 100 µm. **f**, Comparison of stimulus–response curves to sound at night (black line) and day (gray line) of vehicle-treated controls ($n=24$). $P<0.0001$ by extra sum-of-squares *F* test. **g**, Comparison of stimulus–response curves to sound at night (black line) and day (gray line) of BCS-treated larvae ($n=24$). $P=0.32$ by extra sum-of-squares *F* test. **f** and **g** were tested with 6 dpf larvae.

As our imaging experiments establish that the brains of *Cal*^{gw71} mutants are copper deficient, we analyzed rest–activity behaviors in this model. High speed recording of spontaneous swimming during the day show that *Cal*^{gw71} mutants, which are viable[38] and fertile, have comparable locomotion in terms of swimming speed and frequency to the wild-type controls (Supplementary Fig. 13). Characterization of the circadian activities of wild-type larvae and *Cal*^{gw71} mutants (pooled from siblings and cousins), however, revealed distinct differences. Between 4.5 and 6.5 dpf, under a controlled light–dark cycle that mimicked a 14 h day and 10 h night, wild-type larvae cycled in swim activity between higher frequency of swim bouts during the day and lower frequency at night (Supplementary Fig. 14). In contrast, we observed that *Cal*^{gw71} mutants were more active at night and less active during the day than wild-type controls (Fig. 3b and Supplementary Fig. 14).

To further investigate whether dysregulation in brain copper homeostasis triggers additional sleep-related behavioral changes, we studied the acoustic startle responses (ASR)[40] at a range of sound intensities during different phases of the circadian cycle. As in previous studies[41], we observed that wild-type larvae had lower maximal escape responses during day than night (Fig. 3c). This difference is not due to lighting conditions but instead is dependent upon circadian cycles (Supplementary Fig. 15). In contrast, maximal escape responses of *Cal*^{gw71} mutants were indistinguishable between day and night (Fig. 3d). The behavioral differences between wild type and *Cal*^{gw71} mutants were consistent for siblings and cousins (Fig. 3c,d and Supplementary Fig. 16). Together, these results suggest that *Cal*^{gw71} mutants have altered spontaneous swim activities and arousal behaviors during circadian cycles.

To verify that the circadian behavioral changes observed in *Cal*^{gw71} mutants are a direct cause of brain copper deficiency, we reduced brain copper levels through pharmacological interventions. We previously showed through imaging that BCS incubation significantly reduces labile brain copper, and as such, we performed the circadian ASR assay with BCS-treated wild-type larvae and controls (Supplementary Fig. 17). Larvae were treated with 500 µM BCS from 3 to 6 dpf. LA-ICP-MS measurements confirmed that BCS-treated fish had reduced total brain copper compared to wild type (Fig. 3e), but zinc levels remain unchanged (Supplementary Fig. 18). Whereas vehicle-treated controls displayed lower maximal escape responses during day than night (Fig. 3f), BCS-treated larvae exhibited indistinguishable ASR curves during the day and night (Fig. 3g). These data indicate that BCS treatment of wild-type fish recapitulates behavioral deficits in *Cal*^{gw71} mutants, suggesting that maintaining copper homeostasis is essential for modulating behaviors related to circadian cycles and sleep.

Copper transporters are enriched in LC neurons. With data showing that copper is essential for regulating rest–activity and arousal responses, we sought to identify the neural circuitry and molecular targets of how this metal contributes to these fundamental behaviors by directly analyzing expression patterns of genes involved in copper trafficking. We performed in situ hybridization for three major copper transporter genes, *ctr1*, *atp7a* and *atp7b*, in zebrafish larvae. The results show that both *ctr1* and *atp7a* expression patterns are indeed highly spatially regulated (Fig. 4a,b) and that their expression patterns highly resemble that of *dbh* (Fig. 4c), which marks the

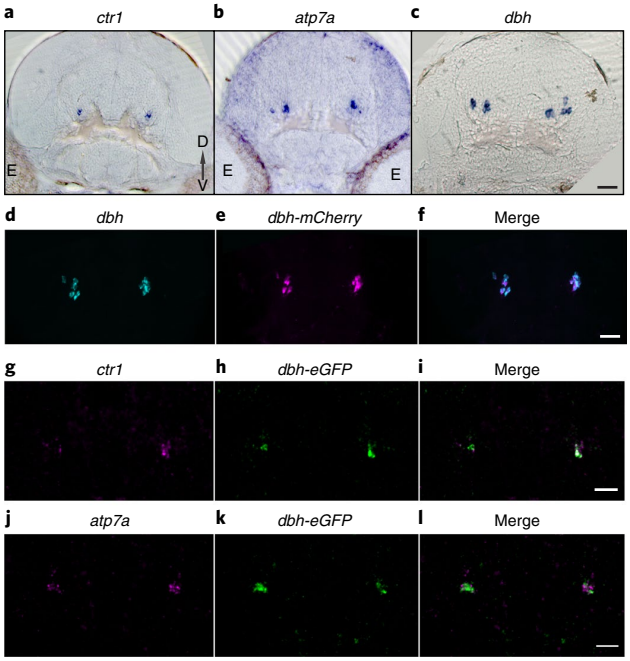

Fig. 4 | Copper transporter gene expression is highly and specifically enriched in LC. a–c, Coronal sections of 3 dpf brains using in situ hybridization to label *ctr1* (**a**), *atp7a* (**b**) and *dbh* (**c**); E, eye; V → D, ventral to dorsal. **d–f**, Dorsal views of a 5 dpf *Tg(dbh:mCherry)* larval brain. **d**, *dbh* mRNA expression detected by fluorescence in situ hybridization. **e**, Anti-mCherry immunostaining. **f**, Merged image from **d** and **e** showing that mCherry is expressed by all *dbh*-positive cells in LC. **g–i**, Horizontal optical sections of a 3 dpf *Tg(dbh:eGFP)* fish labeled with fluorescence in situ hybridization for *ctr1*. **g**, *ctr1* mRNA in magenta. **h**, Anti-GFP labeling showing LC neurons. **i**, Merged image of **g** and **h**. **j–l**, Horizontal optical sections of a 3 dpf *Tg(dbh:eGFP)* fish labeled with fluorescence in situ hybridization for *atp7a*. **j**, *atp7a* mRNA in magenta. **k**, Anti-GFP labeling showing LC neurons. **l**, Merged image of **j** and **k**. Scale bars are 20 μm. Each experiment was independently replicated three times.

LC neurons. This pattern of expression is established by 3 dpf and maintained through adulthood (Supplementary Fig. 19). Similarly, in situ hybridization data from the Allen Mouse Brain Atlas also shows that *Ctr1* (*Slc31a1*) is highly expressed in the mouse LC, but is barely detectable in other brain regions[42]. To confirm the identity of the *ctr1*- and *atp7a*-expressing neurons, we analyzed two transgenic reporter lines, *Tg(dbh:eGFP)* and *Tg(dbh:mCherry)*, in which GFP or mCherry expression is driven by the *dbh* promoter[43]. By using fluorescence in situ hybridization for *dbh*, *ctr1* and *atp7a* mRNA and immunofluorescence staining for GFP or mCherry, we verified that GFP or mCherry expression patterns faithfully reflected the endogenous expression pattern of *dbh* (Fig. 4d–f) and colocalized with *ctr1* (Fig. 4g–i) and *atp7a* (Fig. 4j–l). The results establish that molecular targets for copper import (CTR1), copper-dependent NE synthesis (DBH) and copper export and metalloprotein metalation (ATP7A) are highly and specifically enriched in the LC.

Copper modulates rest–activity cycles through the LC. One of the main roles for the LC in the mammalian brain is to regulate sleep–wake cycles[20,44]. LC is also the brain region with the highest concentration of copper[2,9]. With data showing that LC is the circuitry that contains the highest expression of copper-trafficking genes in the brain, we asked whether LC is necessary for rest–activity cycles regulated by copper homeostasis by using two-photon laser ablation in *Tg(dbh:mCherry)* fish to selectively remove LC cells while leaving the rest of the brain intact.

To determine the time course for ablation and behavior analysis, we characterized the development of LC during the embryonic and larval stage (Supplementary Fig. 20). At 2 dpf, 0–9 LC cell bodies are found per hemi-brain in rhombomere 1. We observed heterogeneity in sibling animals (Supplementary Fig. 21), with little correlation in number of cells between the left and right side (Supplementary Fig. 22) within the same fish, suggesting that epigenetic factors beyond genetic control might contribute to LC cell numbers. In tracking the cells from 2 to 7 dpf, we observed little change in cell count (Supplementary Fig. 23), which indicates cell differentiation is complete and no new LC cells are added to the circuitry. Based on this information, we performed the LC ablation at 3.5–4 dpf and behavioral analysis at 5–7 dpf (Supplementary Fig. 24). Efficacy of the laser ablation was confirmed by imaging after the behavioral analysis (Supplementary Fig. 25).

We first performed circadian ASR analysis. In contrast to wild-type sham controls, which displayed lower maximal responses during the day than night (Fig. 5a), LC-ablated larvae showed elevated ASR maximal responses during the day, which were comparable to maximal responses during the night. When tested for circadian activities (Fig. 5b), between 4.5 and 6.5 dpf, wild-type larvae with an intact LC displayed higher swim activity during the day and lower activity at night under a controlled light–dark cycle (Fig. 5c). In contrast, LC-ablated larvae were more active at night and less active during the day than their LC-intact siblings (Fig. 5c,d and Supplementary Fig. 26), similarly to the copper-deficient *Cal*^{gw71} mutants. The largest differences between the groups were the changes in activity at the dawn transition (Fig. 5d). These data establish that the LC region is necessary for maintaining normal rest–activity cycles in larval zebrafish.

To ask whether rest–activity changes in *Cal*^{gw71} mutants are caused by diminished LC function, we also ablated LC cells in *Cal*^{gw71} mutants. In circadian ASR analysis, LC-ablated *Cal*^{gw71} mutants and sham control *Cal*^{gw71} mutants exhibit similar response curves (Fig. 5e,f). Similarly, circadian activities were also comparable between LC-ablated and sham control *Cal*^{gw71} mutants

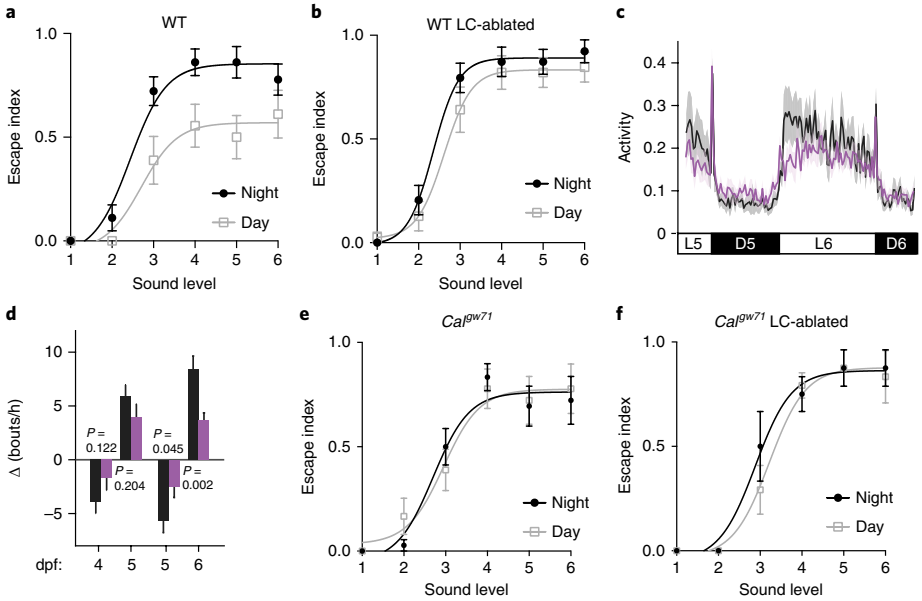

Fig. 5 | LC-NE circuitry mediates copper-regulated behaviors. a, Comparison of stimulus–response curves to sound at night (black line) and daytime (gray line) of wild-type (WT) sham controls ($n=12$). $P<0.0001$ by extra sum-of-squares F test. **b**, Comparison of stimulus–response curves to sound at night (black line) and daytime (gray line) of LC-ablated WT ($n=13$). $P=0.35$ by extra sum-of-squares F test. **c**, Average activity for WT (black, $n=38$) and LC-ablated siblings (purple, $n=34$) from 5.2 to 6.7 dpf. Light (L)/dark (D) cycle is indicated at bottom. For all traces, shaded region is s.e.m. of the population. **d**, Change in frequency of swim bouts recorded in a 3-h period preceding and following light transitions at dusk and dawn. Bars represent mean ± s.e.m. Two-sided Student's t-test. **e**, Comparison of stimulus–response curves to sound at night (black line) and day (gray line) of *Cal*^{gw71} mutant sham controls ($n=12$). $P=0.84$ by extra sum-of-squares F test. **f**, Comparison of stimulus–response curves to sound at night (black line) and day (gray line) of LC-ablated *Cal*^{gw71} mutants ($n=8$). $P=0.56$ by extra sum-of-squares F test. Bars represent mean ± s.e.m.

(Supplementary Fig. 27). The results suggest that rest–activity deficits in *Cal*^{gw71} mutants are caused by compromised LC function.

Copper modulates rest–activity cycles via norepinephrine. To investigate the molecular mechanisms by which copper regulates sleep-related behavior, we used a candidate target approach. Because the LC expresses high levels of the copper-containing enzyme DBH, which is the terminal enzyme in the biosynthesis of NE from DA, we hypothesized that these rest–activity phenotypes could operate through a mechanism whereby reduced DBH activity results in lower NE levels (Fig. 6a). To determine whether DBH activity may cycle with circadian rhythm, we performed reverse transcription and PCR on wild-type larvae, finding that mRNA expression of *dbh* peaked before dawn (Supplementary Fig. 28) whereas the mRNA expression of *atp7a* was constant (Supplementary Fig. 29). The DBH enzyme requires a copper cofactor to catalyze the production of NE; thus, we asked whether a change in copper homeostasis would affect NE production. As expected, we observed a 37% decrease in NE/DA ratio (wild-type larvae: 17.4 ng/ml NE, 2.46 ng/ml DA; *Cal*^{gw71} mutants: 12.9 ng/ml NE, 2.91 ng/ml DA) in copper-deficient *Cal*^{gw71} homozygotes compared to wild-type larvae at 6 dpf (Fig. 6b), consistent with the role of ATP7A in delivering copper to activate DBH for NE synthesis. The expression of DBH was comparable between *Cal*^{gw71} homozygotes and wild-type larvae (Supplementary Fig. 30). This result led to the prediction that LC function would be compromised in the copper-deficient mutant owing to lower levels of NE at synapses than in wild-type congeners through loss of DBH activity.

As a further test of this model, we asked whether atomoxetine, an inhibitor of norepinephrine transporter (NET, also known as Slc6a2)-mediated NE reuptake that prolongs residence of NE in the synapse[45], could rescue the circadian cycle behavioral deficit in the copper-deficient *Cal*^{gw71} mutant. In circadian ASR analysis, atomoxetine-treated *Cal*^{gw71} mutants indeed showed decreased maximal responses during the day (Fig. 6c) and night (Fig. 6d). In contrast, atomoxetine did not change ASR curves in wild type (Fig. 6e,f). Furthermore, we also observed a partial restoration of the rest–activity transition in *Cal*^{gw71} larvae that were exposed from 4.5 dpf to atomoxetine (Fig. 6g,h), as well as a modest decrease in night-time activity. These results provide evidence that both rest and activity states are regulated by NE, likely from a copper-dependent molecular ATP7A–DBH axis. Taken together with the metal imaging and behavioral observations on copper-deficient and LC-deficient fish, the data support a model in which copper enters LC neurons through CTR1 and is loaded into DBH through ATP7A for subsequent NE synthesis and synaptic action, defining a CTR1–ATP7A–DBH–NE molecular pathway for copper-based modulation of sleep-related behavior.

Parallel evolution of norepinephrine and copper pathways. Finally, to identify the key time-point in evolution when NE became a major brain neuromodulator in the CNS, we performed phylogenetic analysis of genes unique to NE biosynthesis and reuptake relative to the other major monoamine neurotransmitters, DA and 5-HT, in parallel to genes involved in copper homeostasis. Specifically, we focused on ATP7A, which loads copper into DBH[23–25] (Fig. 6a and Supplementary Fig. 31). Along these lines, all invertebrates have a single *atp7* gene, whereas vertebrates have two paralogous *atp7* genes, *atp7a* and *atp7b*, which appeared in Agnatha as a result of a gene duplication event in early chordates (Supplementary Fig. 32). Notably, this gene duplication in copper transport is accompanied by appearance of the NE transporter, NET, in Gnathostomata (Supplementary Fig. 31). NET resides at the presynaptic terminal for reuptake of NE from the synaptic cleft. We suggest that these newly acquired genes in both copper homeostasis and NE synthesis

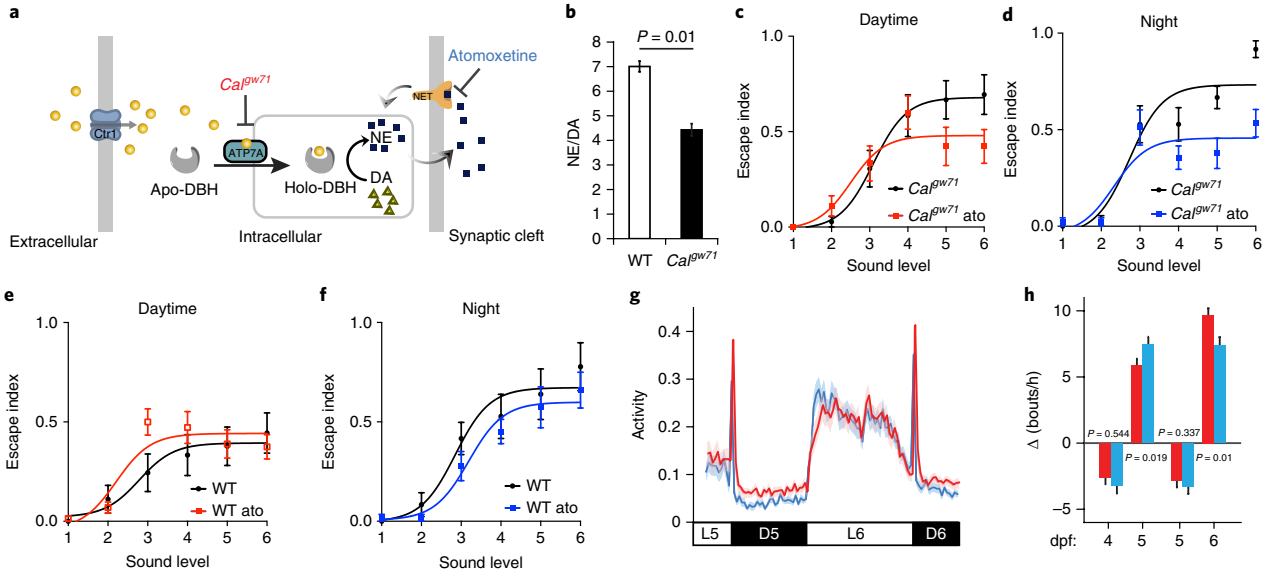

Fig. 6 | Copper transporter gene duplication coincides with the rise of brain NE levels and NE transport in Gnathostomata. a, Schematic drawing of the NE synapse, in which ATP7A metalates DBH with copper. Copper-loaded DBH converts DA to NE inside synaptic vesicles. After NE is released into the synaptic cleft, NET selectively takes up NE back into presynaptic terminals to ensure rapid turnover of NE. **b**, *Cal*^{gw71} mutants exhibit a lower NE-to-DA ratio for 6-dpf larvae. Triplicates of 40 larvae were measured for each group by HPLC with electrochemical detection. Bars represent mean ± s.e.m. Two-sided Student's *t*-test. **c**, Comparison of stimulus–response curves to sound during daytime of *Cal*^{gw71} mutants (black line) and *Cal*^{gw71} mutants treated with 300 nM NET inhibitor atomoxetine (ato; red line) ($n = 15$ for each group). $P < 0.0001$. **d**, Comparison of stimulus–response curves to sound during night of *Cal*^{gw71} mutants (black line) and *Cal*^{gw71} mutants treated with 300 nM NET inhibitor atomoxetine (blue line) ($n = 15$ for each group). $P < 0.0001$. **e**, Comparison of stimulus–response curves to sound during daytime of WT control (black line) and WT treated with 300 nM NET inhibitor atomoxetine (red line) ($n = 15$ for each group). $P = 0.11$. **f**, Comparison of stimulus–response curves to sound during night of WT controls (black line) and WT treated with 300 nM NET inhibitor atomoxetine (blue line) ($n = 15$ for each group). $P = 0.97$. Extra sum-of-squares *F* test (**c**–**f**). **g**, Average activity of *Cal*^{gw71} larvae between 5.2 dpf and 6.7 dpf for those untreated (red, $n = 146$) and treated with 100 nM NET inhibitor atomoxetine (blue, $n = 108$). **h**, Change in swim bout frequency for data in **g**. Two-sided Student's *t*-test. All bars represent mean ± s.e.m.

and transport in early vertebrates may have enabled substantial expansion of NE as a major neurotransmitter.

To provide functional data to support these analyses, we directly measured DA, NE and 5-HT levels in brain extracts of a diverse panel of chordate species around these gene duplication events (Supplementary Fig. 32). In amphioxus (*Branchiostoma lanceolatum*) heads, only DA is observed (180 ng DA per gram wet tissue), with no detectable NE. Further along in evolutionary development, DA is still the dominant monoamine neurotransmitter, at a 7:1 ratio over NE, in lampreys (*Petromyzon marinus*) (142 ng/g DA vs. 20 ng/g NE). Of note, NE levels in lamprey muscle (107 ng/g) are approximately fivefold higher than in brain. Sharks and rays constitute a transition point, wherein one species, dogfish (*Mustelus canis*), has approximately threefold higher NE compared to DA, but two other species (chain catshark, *Scyliorhinus retifer*; ray, *Gymnura micrura*) show much higher levels of DA over NE. Finally, all teleosts tested, namely zebrafish, stickleback (*Gasterosteus aculeatus*) and archerfish (*Toxotes jaculatrix*), possess NE levels that far exceed DA levels in their brains. Taken together, the data indicate that NE, which is biosynthesized by the copper-dependent enzyme DBH, is the newest addition to the group of monoamine neurotransmitters found in the CNS, starting around the gnathostome stage and emerging at the same time as the expansion of the ATP7 copper transporter family.

Discussion

The LC is a unique brain structure, appearing only in vertebrates, that has evolved to be a hub for regulating a diverse array of behaviors spanning sleep, arousal, attention, learning, memory and emotion. As such, a central question in neurobiology is the chemical origin of LC development. At the molecular level, the LC is distinguished as the principal source of NE synthesis in the CNS, mediated exclusively by the copper-dependent enzyme DBH. Recognizing that a central tenet of metals in biology is that they must be acquired because they can neither be created nor destroyed under physiological conditions, we hypothesized that copper itself might represent the most basic chemical origin of LC development.

Major changes of both catecholamine and copper transport systems occurred in parallel after the Cambrian explosion ~540 million years ago. During this period, NE overtook DA as the dominant catecholamine in the CNS, where a small number of LC cells are especially equipped to synthesize steady-state NE levels that far surpass those of the other monoamine neurotransmitters, DA and 5-HT. Through phylogenetic analysis, we identified parallel evolution of genes in copper homeostasis and LC-NE pathways, specifically the duplication of *atp7* into *atp7a* and *atp7b*, coinciding with the rise of the LC-NE system beginning in the gnathostomes. During early vertebrate evolution, it has been suggested that there were two rounds of whole genome duplications, and possibly a third before the split of the rest of the vertebrates from the agnathans[46,47]. The gene encoding ATP7A, which metalates DBH, appeared in Agnatha, potentially resulting from one of these gene duplication events. This major change in copper homeostasis is accompanied by the appearance of the NE transport system for regulating synaptic NE levels through presynaptic reuptake by NET. Notably, NET has not been detected in any species before Gnathostomata. In Gnathostomata, only a partial NET sequence is predicted in the elephant shark (*Callorhinchus milii*) genome. These newly acquired

genes in early vertebrates likely enabled the rise of NE as a major neurotransmitter in Gnathostomata. The functional differentiation between the two ATP7 paralogs[48] might have enabled tissue-specific copper homeostasis that would facilitate diversification of the function of NE and possibly account for evolution of the specialized structure of the LC.

Our findings support the concept that distributions of copper in the CNS are highly spatially and temporally regulated. Indeed, direct metal imaging with LA-ICP-MS, accompanied by a unique pair of fluorescent chemical probes that enable labile copper imaging in the brain in vivo, reveals that copper distributions are developmentally regulated: brain copper levels steadily increase during development, with neuropils and fascicles showing the most marked changes. In contrast, another major transition metal, zinc, is enriched in cell body regions and barely detectable in neuropils. Notably, the spatial resolution afforded by imaging enables detection of specific deficiencies in neurite copper in the brains of a missense mutant of ATP7A, *Cal*^{gw71}, whereas bulk measurements of copper in the entire animal show negligible differences between mutants and wild-type siblings.

We further show that copper is required for normal rest–activity and arousal behaviors in fish. Indeed, LC-NE circuitry has been implicated in sleep and arousal in mammals[20,49] and related behaviors in fish[50], and our data reveal that the LC serves an important role in stabilizing both rest and activity states. Since *dbh* gene transcription reaches peak levels just before dawn, production of the copper-dependent DBH protein before waking may be particularly affected by impaired copper homeostasis, leading to impaired NE synthesis. In line with this reasoning, we found that *Cal*^{gw71} ATP7A mutants exhibiting brain copper deficiency had pronounced and specific defects in the rest–activity transition, despite being indistinguishable from their wild-type siblings in gross morphology, growth and fertility. The copper-dependent rest–activity defect can be rescued pharmacologically using NET inhibitors that increase synaptic NE levels, linking the need for copper to DBH activity and NE production and supporting a model whereby copper homeostasis is indeed essential for LC function through a CTR1–ATP7A–DBH–NE molecular pathway.

This work establishing copper as an elemental chemical origin of the LC and regulator of LC-mediated sleep-related behavior has broader implications, as clinical copper dysregulation can cause a wide range of neurological symptoms beyond sleep disorders, including depression, intellectual disability and neurodegeneration[20]. For example, in the copper-dependent genetic disorder Wilson's disease, 50% of the patients are diagnosed with neurological symptoms, with severity uncorrelated with the severity of the copper-dependent liver damage[39]. More complex neurodegenerative disorders, including Alzheimer's, Parkinson's and Huntington's diseases, along with ALS and autism, involve alterations in copper homeostasis and thus motivate further investigations of the metallophysiology/metallopathology interface for both fundamental research and new therapeutic interventions.

Methods

Methods, including statements of data availability and any associated accession codes and references, are available at https://doi.org/10.1038/s41589-018-0062-z.

Received: 28 November 2017; Accepted: 19 March 2018;
Published online: 4 June 2018

References

1. Bush, A. I. Metals and neuroscience. *Curr. Opin. Chem. Biol.* **4**, 184–191 (2000).
2. Que, E. L., Domaille, D. W. & Chang, C. J. Metals in neurobiology: probing their chemistry and biology with molecular imaging. *Chem. Rev.* **108**, 1517–1549 (2008).
3. Barnham, K. J., Masters, C. L. & Bush, A. I. Neurodegenerative diseases and oxidative stress. *Nat. Rev. Drug Discov.* **3**, 205–214 (2004).
4. Kaler, S. G. ATP7A-related copper transport diseases-emerging concepts and future trends. *Nat. Rev. Neurol.* **7**, 15–29 (2011).
5. Madsen, E. & Gitlin, J. D. Copper and iron disorders of the brain. *Annu. Rev. Neurosci.* **30**, 317–337 (2007).
6. Zlatic, S., Comstra, H. S., Gokhale, A., Petris, M. J. & Faundez, V. Molecular basis of neurodegeneration and neurodevelopmental defects in Menkes disease. *Neurobiol. Dis.* **81**, 154–161 (2015).
7. Duncan, C. & White, A. R. Copper complexes as therapeutic agents. *Metallomics* **4**, 127–138 (2012).
8. Lutsenko, S., Bhattacharjee, A. & Hubbard, A. L. Copper handling machinery of the brain. *Metallomics* **2**, 596–608 (2010).
9. Prohaska, J. R. Functions of trace elements in brain metabolism. *Physiol. Rev.* **67**, 858–901 (1987).
10. Warren, P. J., Earl, C. J. & Thompson, R. H. The distribution of copper in human brain. *Brain* **83**, 709–717 (1960).
11. Zecca, L. et al. The role of iron and copper molecules in the neuronal vulnerability of locus coeruleus and substantia nigra during aging. *Proc. Natl Acad. Sci. USA* **101**, 9843–9848 (2004).
12. German, D. C. et al. Disease-specific patterns of locus coeruleus cell loss. *Ann. Neurol.* **32**, 667–676 (1992).
13. Braak, H. & Del Tredici, K. Where, when, and in what form does sporadic Alzheimer's disease begin? *Curr. Opin. Neurol.* **25**, 708–714 (2012).
14. Cotruvo, J. A. Jr, Aron, A. T., Ramos-Torres, K. M. & Chang, C. J. Synthetic fluorescent probes for studying copper in biological systems. *Chem. Soc. Rev.* **44**, 4400–4414 (2015).
15. Nevitt, T., Ohrvik, H. & Thiele, D. J. Charting the travels of copper in eukaryotes from yeast to mammals. *Biochim. Biophys. Acta* **1823**, 1580–1593 (2012).
16. Robinson, N. J. & Winge, D. R. Copper metallochaperones. *Annu. Rev. Biochem.* **79**, 537–562 (2010).
17. O'Halloran, T. V. & Culotta, V. C. Metallochaperones, an intracellular shuttle service for metal ions. *J. Biol. Chem.* **275**, 25057–25060 (2000).
18. Banci, L. et al. Affinity gradients drive copper to cellular destinations. *Nature* **465**, 645–648 (2010).
19. Lutsenko, S., Barnes, N. L., Bartee, M. Y. & Dmitriev, O. Y. Function and regulation of human copper-transporting ATPases. *Physiol. Rev.* **87**, 1011–1046 (2007).
20. Aston-Jones, G. & Waterhouse, B. Locus coeruleus: from global projection system to adaptive regulation of behavior. *Brain Res.* **1645**, 75–78 (2016).
21. Sara, S. J. The locus coeruleus and noradrenergic modulation of cognition. *Nat. Rev. Neurosci.* **10**, 211–223 (2009).
22. Moret, C. & Briley, M. The importance of norepinephrine in depression. *Neuropsychiatr. Dis. Treat.* **7**, 9–13 (2011). (Suppl. 1).
23. Kaufman, S. & Friedman, S. Dopamine-β-hydroxylase. *Pharmacol. Rev.* **17**, 71–100 (1965).
24. Mangold, J. B. & Klinman, J. P. Mechanism-based inactivation of dopamine β-monooxygenase by β-chlorophenethylamine. *J. Biol. Chem.* **259**, 7772–7779 (1984).
25. Ash, D. E., Papadopoulos, N. J., Colombo, G. & Villafranca, J. J. Kinetic and spectroscopic studies of the interaction of copper with dopamine β-hydroxylase. *J. Biol. Chem.* **259**, 3395–3398 (1984).
26. Kim, B. E., Nevitt, T. & Thiele, D. J. Mechanisms for copper acquisition, distribution and regulation. *Nat. Chem. Biol.* **4**, 176–185 (2008).
27. Scatton, B., Javoy-Agid, F., Rouquier, L., Dubois, B. & Agid, Y. Reduction of cortical dopamine, noradrenaline, serotonin and their metabolites in Parkinson's disease. *Brain Res.* **275**, 321–328 (1983).
28. Hornby, P. J. & Piekut, D. T. Immunoreactive dopamine β-hydroxylase in neuronal groups in the goldfish brain. *Brain Behav. Evol.* **32**, 252–256 (1988).
29. Ekström, P., Reschke, M., Steinbusch, H. & van Veen, T. Distribution of noradrenaline in the brain of the teleost *Gasterosteus aculeatus* L.: an immunohistochemical analysis. *J. Comp. Neurol.* **254**, 297–313 (1986).
30. Parent, A. Functional anatomy and evolution of monoaminergic systems. *Am. Zool.* **24**, 783–790 (1984).
31. Hirayama, T., Van de Bittner, G. C., Gray, L. W., Lutsenko, S. & Chang, C. J. Near-infrared fluorescent sensor for in vivo copper imaging in a murine Wilson disease model. *Proc. Natl Acad. Sci. USA* **109**, 2228–2233 (2012).
32. Heffern, M. C. et al. In vivo bioluminescence imaging reveals copper deficiency in a murine model of nonalcoholic fatty liver disease. *Proc. Natl Acad. Sci. USA* **113**, 14219–14224 (2016).
33. Hare, D. J., New, E. J., de Jonge, M. D. & McColl, G. Imaging metals in biology: balancing sensitivity, selectivity and spatial resolution. *Chem. Soc. Rev.* **44**, 5941–5958 (2015).
34. Ackerman, C. M., Lee, S. & Chang, C. J. Analytical methods for imaging metals in biology: from transition metal metabolism to transition metal signaling. *Anal. Chem.* **89**, 22–41 (2017).
35. Colburn, R. W. & Maas, J. W. Adenosine triphosphate–metal–norepinephrine ternary complexes and catecholamine binding. *Nature* **208**, 37–41 (1965).
36. Sato, M., Ohtomo, K., Daimon, T., Sugiyama, T. & Iijima, K. Localization of copper to afferent terminals in rat locus ceruleus, in contrast to mitochondrial copper in cerebellum. *J. Histochem. Cytochem.* **42**, 1585–1591 (1994).
37. Gaier, E. D., Eipper, B. A. & Mains, R. E. Copper signaling in the mammalian nervous system: synaptic effects. *J. Neurosci. Res.* **91**, 2–19 (2013).

38. Madsen, E. C. & Gitlin, J. D. Zebrafish mutants calamity and catastrophe define critical pathways of gene-nutrient interactions in developmental copper metabolism. *PLoS Genet.* **4**, e1000261 (2008).
39. Zimbrean, P. C. & Schilsky, M. L. Psychiatric aspects of Wilson disease: a review. *Gen. Hosp. Psychiatry* **36**, 53–62 (2014).
40. Pantoja, C. et al. Neuromodulatory regulation of behavioral individuality in zebrafish. *Neuron* **91**, 587–601 (2016).
41. Chen, S. et al. Light-dependent regulation of sleep and wake states by prokineticin 2 in zebrafish. *Neuron* **95**, 153–168.e156 (2017).
42. Lein, E. S. et al. Genome-wide atlas of gene expression in the adult mouse brain. *Nature* **445**, 168–176 (2007).
43. Zhu, S. et al. Activated ALK collaborates with MYCN in neuroblastoma pathogenesis. *Cancer Cell* **21**, 362–373 (2012).
44. Deisseroth, K. Circuit dynamics of adaptive and maladaptive behaviour. *Nature* **505**, 309–317 (2014).
45. Caballero, J. & Nahata, M. C. Atomoxetine hydrochloride for the treatment of attention-deficit/hyperactivity disorder. *Clin. Ther.* **25**, 3065–3083 (2003).
46. Dehal, P. & Boore, J. L. Two rounds of whole genome duplication in the ancestral vertebrate. *PLoS Biol.* **3**, e314 (2005).
47. Panopoulou, G. & Poustka, A. J. Timing and mechanism of ancient vertebrate genome duplications — the adventure of a hypothesis. *Trends Genet.* **21**, 559–567 (2005).
48. Dmitriev, O. et al. Solution structure of the N-domain of Wilson disease protein: distinct nucleotide-binding environment and effects of disease mutations. *Proc. Natl Acad. Sci. USA* **103**, 5302–5307 (2006).
49. Li, S. B., Jones, J. R. & de Lecea, L. Hypocretins, neural systems, physiology, and psychiatric disorders. *Curr. Psychiatry Rep.* **18**, 7 (2016).
50. Singh, C., Oikonomou, G. & Prober, D. A. Norepinephrine is required to promote wakefulness and for hypocretin-induced arousal in zebrafish. *Elife* **4**, e07000 (2015).

Acknowledgements

We thank A. T. Look (Dana-Farber Cancer Institute) and J. Gitlin (Marine Biological Laboratory) for providing plasmids and transgenic fish lines, C. Miller (University of California, Berkeley) and R. Segev (Ben Gurion University of the Negev) for providing fish samples, and R. Feng and R. Fish for assistance with pilot experiments. We thank the NIH (GM79465 to C.J.C. and PN2EY018241 to E.Y.I.) for providing funding for this work. C.J.C. is an Investigator of the Howard Hughes Medical Institute and a CIFAR Senior Fellow. C.M.A. was partially supported by a Hertz Foundation Graduate Fellowship and a Chemical Biology Training Grant from the NIH (T32 GM066698). Experiments at the CRL Molecular Imaging Center were supported by the Helen Wills Neuroscience Institute.

Author contributions

T.X. and C.J.C. designed research; T.X., C.M.A., E.C.C. and A.H. performed imaging and behavioral assays; T.X., C.M.A. and B.T. performed copper imaging and analysis assays; S.J. and J.C. synthesized and characterized fluorescent copper probes; T.X. and C.S.L. conducted in situ hybridization and IHC assays; T.X., C.M.A., E.C.C. and C.J.C. wrote the manuscript; E.Y.I. provided valuable input on the manuscript.

Competing interests

The authors declare no competing financial interests.

Additional information

Supplementary information is available for this paper at https://doi.org/10.1038/s41589-018-0062-z.

Reprints and permissions information is available at www.nature.com/reprints.

Correspondence and requests for materials should be addressed to C.J.C.

Publisher's note: Springer Nature remains neutral with regard to jurisdictional claims in published maps and institutional affiliations.

Methods

Synthesis of CF4 and Ctrl-CF4-S2. See Supplementary Note.

Zebrafish lines. Zebrafish of the AB and TL strains were raised and bred at 28.5 °C on a 14 h light/10 h dark cycle. Embryos were produced by natural crosses and staged by hours or days post fertilization (hpf or dpf, respectively) following AUP in compliance with zebrafish ethical regulations and approved by the UC Berkeley ACUC. Embryos were raised in copper-free E3 or egg water (60 µg/ml Instant Ocean Sea Salt in distilled water). Instant Ocean Sea Salt contains approximately 1.8 µmol/kg of copper[51]. Designations of mutant and transgenic lines adhered to nomenclature rules set according to http://zfin.org/. The following mutants or transgenic lines were used: *Calamity*^{gw71} mutants (*Cal*^{gw71})[38], *nacre* (*mitfa*$^{-/-}$) mutants[52], *Tg(elavl3:GCaMP5)*[53], *Tg(dbh:mCherry)* and *Tg(dbh:eGFP)*[43]. Genotyping of *Cal*^{gw71} mutants was carried out as described previously[38].

In vivo labeling. Zebrafish embryos in *nacre* background were incubated in 10 µM CF4 or Ctrl-CF4-S2 with 1% DMSO in E3 solution overnight. Embryos were washed, embedded in 2% low-melting agarose, and imaged 3 dpf.

Fluorescence microscopy imaging. Larvae were embedding in 2% agarose and imaged by laser scanning confocal microscopy (Zeiss, using a 20×, NA 1.0 water-immersion objective) at 0.5 µm per step. *z*-stacks were obtained at 1,024 p with a pinhole of 1 Airy unit at 488 nm excitation. Channels for 488 nm, 561 nm and transmitted light images were acquired simultaneously.

Two-photon laser ablation assays. For behavioral studies in LC-ablated animals, *Tg(dbh-mCherry; elavl3:GCaMP5)* larvae were mounted in agarose at 3 dpf, and LC cells were bilaterally removed by two-photon ablation on a Zeiss LSM 880 confocal microscope. The 800-nm ablation laser (Coherent Chameleon Vision) was rastered over LC somata guided by mCherry fluorescence, and the progress of the ablation was monitored by simultaneously imaging Ca^{2+} responses from GCaMP5 and microcavitation with transmitted light. In this way, LC cells were selectively destroyed with very little collateral damage. Larvae were unmounted and allowed to recover for at least 24 h before behavior experiments. LC-intact siblings were subjected to the same rearing conditions to control for rate of development. Following behavior experiments, ablated animals were reimaged to confirm complete loss of LC.

Liquid sample ICP-MS. Fish were euthanized in tricaine or ice following a standard protocol. Tissues were quickly harvested and weighed, then digested in 1 mL trace-metals-grade concentrated nitric acid per 100 mg of tissue, at room temperature on a rotator in 1.5 mL tubes (Sarstedt). Digested samples were diluted in 2% nitric acid with 1 p.p.m. gallium solution as an internal control and analyzed with iCAP-Qc ICP-MS (Thermo Fisher).

Laser ablation inductively coupled plasma mass spectrometry (LA-ICP-MS). Zebrafish embryos were raised in Instant Ocean to 2, 4 or 6 days post fertilization (dpf). Embryos were euthanized and immediately embedded in Optimal Cutting Temperature (OCT) mounting medium (Tissue Tek) in cryomolds (Tissue Tek). The embedded embryos were immediately frozen in a dry ice/isopentane bath and stored at −80 °C until sectioning. For 4–18 h before sectioning, the embedded embryos were equilibrated to −20 °C. The embryos were sectioned into 20-µm slices using Leica CM1950 and adhered to Superfrost slides (Thermo Fisher). The slices were air-dried and stored at room temperature until analysis. Laser ablation was performed on an NWR213 laser with a TV2 sample chamber (ESI, Bozeman, MT) using the following parameters: spot size: 6 µm; fluence: 2.3 J cm^{-2}; stage speed: 15 µm s^{-1}; firing rate: 20 Hz; He flow: 800 mL min^{-1}; pattern spacing: 6 µm. Using these parameters, the tissue was fully ablated but the glass slide remained undamaged. The ablated material was introduced by gas flow into an iCAP-Qc ICP-MS (Thermo Fisher) and analyzed for ^{63}Cu or ^{66}Zn content using a 0.4 s dwell time in standard acquisition mode. The resulting mass spectrometry traces and laser log files were processed in Igor Pro using the Iolite application. The trace elements data reduction scheme was used in semi-quantitative mode using ^{63}Cu or ^{66}Zn as the reference trace and a custom matrix-matched standard to convert mass spectrometer counts to metal concentration.

Preparation of matrix-matched LA-ICP-MS standards. Salmon muscle (30 mL of packed tissue) was digested by adding 10 mL of protease solution (0.25% trypsin, 10 mM EDTA, 0.1× PBS) and 48 µL of Collagenase P (100 mg mL^{-1} in HBSS) in a 50-mL plastic conical tube. The solution was mixed with a plastic spatula (to minimize metal contamination) and incubated at 28 °C for 4 h with periodic mixing. The tissue was stored at 4 °C overnight. The next day, the tissue was warmed to 28 °C for an additional 6 h of digestion and homogenized in a Dounce homogenizer using ten passes until the tissue was gooey and smooth. The tissue was separated into 500 µL aliquots in 1.5 mL Sarstedt tubes and frozen at −20 °C until metal addition. A solution of $CuCl_2$, $ZnCl_2$, iron(III) citrate, $CaCl_2$, $MgCl_2$ and KCl (10,000 p.p.m. each) was prepared in water. Dilutions of 5,000, 1,000, 500, 100, 50 and 10 p.p.m. were made in water. Each dilution was mixed 1:10 with an aliquot of tissue (50 µL metal mixture per 500 µL tissue) and mixed with a hand-held mechanical homogenizer. To remove bubbles, the standards were centrifuged at 16,000 *g* at room temperature for 2 h. Any resulting supernatant was removed, and the vials were frozen in a dry ice/isopentane bath and stored at −80 °C until sectioning. Before sectioning, the standards were cut in half vertically. One half was sectioned into-20 µm slices using a cryostat (Leica CM1950) and adhered to Superfrost slides (Thermo Fisher), air-dried, and stored at room temperature until analysis. The other half was divided into three parts for liquid ICP-MS analysis. The samples for liquid analysis were weighed in 1.5 mL tubes (Sarstedt) and combined 1:1 (w/v) with concentrated nitric acid (BDH Aristar Ultra). After overnight incubation at room temperature, samples were diluted into 2% HNO_3 (prepared from concentrated acid in milliQ water) and doped with a gallium internal standard (Inorganic Ventures, 20 p.p.b. final concentration). The metal content was determined by measuring ^{63}Cu and ^{66}Zn using a Thermo Fisher iCAP-Qc ICP-MS in kinetic energy discrimination (KED) mode with the helium flow set to 4.426 mL min^{-1}. Measurements were normalized to a standard curve of known metal concentrations doped with 20 p.p.b. gallium. The standard curve was diluted from CMS-5 (Inorganic Ventures).

Rest–activity and acoustic startle response assays. Embryos in AB strain background were raised in E3 under a 14 h light/10 h dark light cycle at 28.6 °C until 4 dpf. Larvae with fully inflated swim bladders were then transferred individually into 48-well plates in 900 µL of E3, with or without drug treatment, and placed in a light-controlled imaging arena maintained under the same 14 h light/10 h dark with ambient light on between 9:00 a.m. and 11:00 p.m. Recording was conducted using a custom-built apparatus. Film resolution of 1,388 × 1,240 p corresponded to 140 × 140 p per well. Larvae were filmed between 4.5 and 6.5 dpf for 1 min (1 fps) at intervals of 4.5 min for rest–activity assays.

For acoustic startle response assay, sound was delivered by two speakers (Visaton SC5.9) coupled to the multi-well plate via the plate-holder platform and driven by a 15 W amplifier. The acoustic stimuli were 900 Hz square waves of ~3 ms duration, ranging across six different volume levels of approximately 68 dB, 73.5 dB, 79 dB, 84.5 dB, 90 dB and 95.5 dB. Each of the six volumes were randomly delivered three times per level in the morning (~10 a.m.) and night (~2 a.m.). Larvae were filmed at 30 fps.

Behavioral analysis. Activity was quantified by summing pixel changes between frames using custom scripts in Fiji/ImageJ and Matlab (MathWorks). Cohort mean activity traces were obtained from mean of normalized individual activity. Animals with no inflated swim bladder or no activity (<10% population) were excluded from analysis. An escape event was calculated using the difference in pixel values between frames. An acoustic startle response was counted if the difference of the summated pixel values from the two frames immediately following the stimulus was statistically higher ($P < 0.01$, two-sample *t*-test) than the distribution of pixel-change values taken from the non-escape portion of spontaneous activity in the movies. This analysis method was confirmed by visual inspection of the behavioral movies. Data used are pooled from fish bred over three generations. Wild-type controls are either genotyped siblings or cousins of the *Cal*^{gw71} mutants.

In situ hybridization assays. A fragment of *dbh* was amplified from cDNA by PCR and cloned into pCR2.1 vector. The following primers were used: 5′-CTCCTCGGGCATTCGTTTAT-3″ and 5′-CCTCTGTAGGGCTGTCATTATTAG-3′. Plasmids containing *ctr1* (*slc31a1*) and *atp7a* cDNA fragments were kindly provided by Jonathan Gitlin. In situ hybridization was performed as described previously[54]. Fragments of *ctr1*, *atp7a* and *dbh* were used to generate respective sense and antisense riboprobes with digoxigenin-labeled UTP. Probes were hydrolyzed to yield 200-base fragments. Embryos or larvae were sectioned in gelatin/albumin at 20 µm coronally on a vibratome (Leica). For fluorescence in situ hybridization, anti-DIG POD (Roche) was used at 1:400 dilution followed by tyramide amplification.

Immunohistochemistry. Immunohistochemistry stainings were performed as described previously[54]. Anti-GFP (Invitrogen, A-6455) was used at 1:4,000 for wholemount immunohistochemistry; anti-mCherry (Chemicon, AB356482) was used at 1:1,200 for frozen-section immunohistochemistry. The following secondary antibodies were used: goat anti-rabbit Alexa Fluor 488 (Thermo Fisher, A-11008) was used 1:250; goat anti-rabbit Alexa Fluor 647 (Thermo Fisher, A-21244) was used 1:250.

Real-time PCR analysis. Triplicates of 30 larvae from 5 dpf to 6 dpf were collected every 4 h and frozen in RNAlater (Thermo Fisher). RNA was extract with RNAasy Plus (Qiagen), quantified and then reverse-transcribed with iScript (Bio-Rad). Real-time PCR was performed using iQ SYBRGreen following the standard protocol on a CFX Real-Time system (Bio-Rad). The following primers were used:

dbh: 5′-CTTGGGCTGGTCTACACTC-3′; 5′-TGGGAGGCAAAGATGTGTATG-3′

atp7a: 5′- TGACCTGTGGCTCCTGTGTA-3′; 5′-CTGGTGTTGATGTAGCGTTTG-3′

ctr1: 5′- GTGAACGTGCGCTACAACTC-3′; 5′- CCACCACTTGGATGATGTGA-3′
EF1a (*eef1a1/1*): 5′- CTGGAGGCCAGCTCAAACAT-3′; 5′- ATCAAGAAGAGTAGTACCGCTAGCATTAC-3′
b-actin (*actb1*): 5′- CGAGCTGTCTTCCCATCC A-3′; 5′- TCACCAACGTAGCTGTCTTTCTG-3′

Phylogenetic analysis. The trees were built based on ensemble methods[55]. Data were exported and plotted with Matlab.

Catecholamine analysis. Amphioxus, shark and ray brain samples were purchased from Marine Biological Laboratory and Gulf Specimen. Sticklebacks were kindly provided by Craig Miller. Archer fish were kindly provided by Ronen Segev. Brains were quickly dissected, weighed, and homogenized in 0.1 M PCA solution. After centrifuging, supernatants were analyzed by HPLC-ECD for norepinephrine (NE) and dopamine (DA) or LC/MS/MS for serotonin (5-HT) by BASi.

Briefly, to detect serotonin from fish tissue extract by LC/MS/MS, glycinexylidide was added to the clear fish tissue extract as internal standard before injection. After vortex-mixing and centrifugation, the sample was injected into an LC-MS/MS system using a PFP column with a gradient water/acetonitrile/formic acid mobile phase. NE and DA were detected from fish tissue extract by LC/EC. 3,4-Dihydroxybenzylamine was added to the clear fish tissue extract as internal standard before the injection. After vortex-mixing and centrifugation, the sample was injected into an LC/EC system using a Gemini C18 column with a EDTA/SDS/phosphate buffer mobile phase.

Statistics and reproducibility. Statistical tests were conducted using GraphPad Prism7 and Matlab (2016a). In Fig. 6, bars represent mean ± s.e.m. In Fig. 6g, shaded region is s.e.m. of population.

Reporting summary. Further information on experimental design is available in the Nature Research Reporting Summary linked to this article.

Code availability. Code supporting this study is available upon reasonable request.

Data availability. The data that support the findings of this study are available from the corresponding authors upon reasonable request.

References

51. Atkinson, M. J. & Bingman, C. Elemental composition of commercial seasalts. *J. Aquaricult. Aquat. Sci.* **VIII**, 39–43 (1998).
52. Lister, J. A., Robertson, C. P., Lepage, T., Johnson, S. L. & Raible, D. W. *nacre* encodes a zebrafish microphthalmia-related protein that regulates neural-crest-derived pigment cell fate. *Development* **126**, 3757–3767 (1999).
53. Ahrens, M. B., Orger, M. B., Robson, D. N., Li, J. M. & Keller, P. J. Whole-brain functional imaging at cellular resolution using light-sheet microscopy. *Nat. Methods* **10**, 413–420 (2013).
54. Xiao, T. & Baier, H. Lamina-specific axonal projections in the zebrafish tectum require the type IV collagen Dragnet. *Nat. Neurosci.* **10**, 1529–1537 (2007).
55. Vilella, A. J. et al. EnsemblCompara GeneTrees: complete, duplication-aware phylogenetic trees in vertebrates. *Genome Res.* **19**, 327–335 (2009).

nature research

Corresponding author(s): Christopher J Chang

☐ Initial submission ☐ Revised version ☑ Final submission

Life Sciences Reporting Summary

Nature Research wishes to improve the reproducibility of the work that we publish. This form is intended for publication with all accepted life science papers and provides structure for consistency and transparency in reporting. Every life science submission will use this form; some list items might not apply to an individual manuscript, but all fields must be completed for clarity.

For further information on the points included in this form, see Reporting Life Sciences Research. For further information on Nature Research policies, including our data availability policy, see Authors & Referees and the Editorial Policy Checklist.

Experimental design

1. Sample size

Describe how sample size was determined.

The sample size was chosen based on feasibility and literature precedence for similar experiments. Sample sizes are reported in figure legends.

2. Data exclusions

Describe any data exclusions.

Larvae without inflated swimming bladder or no locomotor activity were excluded based on literature precedence for similar experiments

3. Replication

Describe whether the experimental findings were reliably reproduced.

All experiments contain minimum of biological replicates and technical replicates. All results from replicates are consistent.

4. Randomization

Describe how samples/organisms/participants were allocated into experimental groups.

Zebrafish animals were collected from natural crosses, pooled and distributed into multiwell plates, genotyped post recording.

5. Blinding

Describe whether the investigators were blinded to group allocation during data collection and/or analysis.

Data analysis were carried out with Matlab scripts or instrument programs. Therefore, investigators were not blinded to group allocation or analysis of the outcome.

Note: all studies involving animals and/or human research participants must disclose whether blinding and randomization were used.

6. Statistical parameters

For all figures and tables that use statistical methods, confirm that the following items are present in relevant figure legends (or in the Methods section if additional space is needed).

n/a	Confirmed
☐	☑ The exact sample size (*n*) for each experimental group/condition, given as a discrete number and unit of measurement (animals, litters, cultures, etc.)
☐	☑ A description of how samples were collected, noting whether measurements were taken from distinct samples or whether the same sample was measured repeatedly
☐	☑ A statement indicating how many times each experiment was replicated
☐	☑ The statistical test(s) used and whether they are one- or two-sided (note: only common tests should be described solely by name; more complex techniques should be described in the Methods section)
☐	☑ A description of any assumptions or corrections, such as an adjustment for multiple comparisons
☐	☑ The test results (e.g. *P* values) given as exact values whenever possible and with confidence intervals noted
☐	☑ A clear description of statistics including central tendency (e.g. median, mean) and variation (e.g. standard deviation, interquartile range)
☐	☑ Clearly defined error bars

See the web collection on statistics for biologists for further resources and guidance.

Software

Policy information about availability of computer code

7. Software

Describe the software used to analyze the data in this study.	Data was analyzed with Fiji version1.0/ImageJ (NIH), Matlab 20016a and Graphpad Prism7.

For manuscripts utilizing custom algorithms or software that are central to the paper but not yet described in the published literature, software must be made available to editors and reviewers upon request. We strongly encourage code deposition in a community repository (e.g. GitHub). *Nature Methods* guidance for providing algorithms and software for publication provides further information on this topic.

Materials and reagents

Policy information about availability of materials

8. Materials availability

Indicate whether there are restrictions on availability of unique materials or if these materials are only available for distribution by a for-profit company.	All materials are available upon request.

9. Antibodies

Describe the antibodies used and how they were validated for use in the system under study (i.e. assay and species).	All antibodies used are from commercial sources, verified by manufacture quality control. Catalog numbers described in methods section.

10. Eukaryotic cell lines

a. State the source of each eukaryotic cell line used.	HEK293T cells were obtained from ATCC through UC Berkeley Cell Culture Facility.
b. Describe the method of cell line authentication used.	Cells were authenticated by ATCC and UC Berkeley Cell Culture Facility.
c. Report whether the cell lines were tested for mycoplasma contamination.	Cells were tested for myoplasma by UC Berkeley Cell Culture Facility.
d. If any of the cell lines used are listed in the database of commonly misidentified cell lines maintained by ICLAC, provide a scientific rationale for their use.	No commonly misidentified cell lines were used.

Animals and human research participants

Policy information about studies involving animals; when reporting animal research, follow the ARRIVE guidelines

11. Description of research animals

Provide details on animals and/or animal-derived materials used in the study.	Zebrafish Embryos or larvae from 2-6 days post fertilization of the AB and TL strains were used in this study. Sex determination is not applicable at these stages. The following mutants or transgenic lines were used: Calamitygw71 mutants (Calgw71), nacre/mitfa(-/-) mutants, Tg(elavl3:GCaMP5), Tg(dbh:mCherry), and Tg(dbh:eGFP).

Policy information about studies involving human research participants

12. Description of human research participants

Describe the covariate-relevant population characteristics of the human research participants.	The study did not involve human research participants.